ACS APPLIED MATERIALS & INTERFACES

Research Article

www.acsami.org

Enhanced Photocatalytic H_2 Generation on Cadmium Sulfide Nanorods with Cobalt Hydroxide as Cocatalyst and Insights into Their Photogenerated Charge Transfer Properties

Li J. Zhang,[†] Rui. Zheng,[†] Shuo. Li,[†] Bing K. Liu,[†] De J. Wang,[†,§] Ling L. Wang,*[,‡] and Teng F. Xie*[,†]

[†]State Key Laboratory of Theoretical and Computational Chemistry, College of Chemistry, Jilin University, Changchun 130012, People's Republic of China

[‡]State Key Laboratory of Supramolecular Structure and Materials, College of Chemistry, Jilin University, Changchun 130012, People's Republic of China

[§]Department of Chemistry, Tsinghua University, Beijing 100084, People's Republic of China

Supporting Information

ABSTRACT: Cobalt hydroxide/cadmium sulfide composite was prepared using an easy coprecipitation strategy. The field emission scanning electron microscopy (FESEM) and transmission electron microscopy (TEM) confirmed that $Co(OH)_2$ nanometer particles were modified on CdS. Even without noble-metal cocatalyst, the photocatalytic H_2 evolution over CdS after $Co(OH)_2$ loaded was evidently increased. The most excellent $Co(OH)_2$ of 6.8 mol %, resulted in a H_2 generation rate of 61 μmol h^{-1} g^{-1}, which exceeded that of pure CdS by a factor of 41 times. Surface photovoltage (SPV) and surface photocurrent (SPC) investigations revealed that the photogenerated electrons could be captured by the loaded $Co(OH)_2$ nanoparticles. The interface formed between $Co(OH)_2$ and CdS is vital to the enhancement of photocatalytic H_2 generation. Electrochemical measurement results indicated that another reason for the enhanced photocatalytic activity of $Co(OH)_2$/CdS catalyst is that $Co(OH)_2$ has outstanding H_2 generation activity.

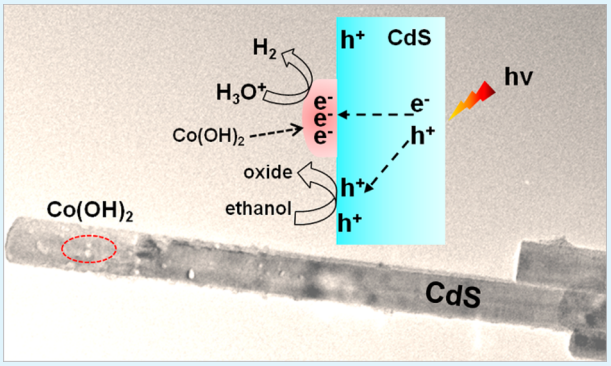

KEYWORDS: *$Co(OH)_2$, photocatalytic H_2 evolution, surface photovoltage, photogenerated charge transfer, CdS, surface photocurrent*

INTRODUCTION

With excessive consumption of fossil fuels and growing environmental pollution, solutions to energy, and environmental issues have become urgently important topics nowadays. For resolving energy crisis and environment problems, photocatalytic H_2 evolution using photocatalysts of semiconductors has been considered as an attractive way.[1−5] CdS is an attractive semiconductor for H_2 evolution and is widely studied for its narrow band gap and sufficiently negative conduction band potential.[6−9] Traditionally, for improving the photocatalytic H_2 generation efficiency over CdS, noble metals (Pt, Rh, and Pd) are essential cocatalysts.[10−12] However, noble metals are scarce and of high-cost. Therefore, it is vital to find highly efficient and low-cost cocatalysts to replace noble metals for sustainable development.[13,14] Zong and co-workers thought that MoS_2 and WS_2 are outstanding cocatalysts of CdS. The MoS_2[15] and WS_2[16] loaded could increase the H_2 generation rate for CdS. What is more, our studies indicated that the H_2 generation rate of $Zn_{0.8}Cd_{0.2}S$ was remarkably improved by CuS loaded.[17] Cobalt hydroxide is an earth-abundant and promising transition metal hydroxide, which has been recently used in supercapacitors, batteries, and photocatalysts.[18−20] However, as far as we know, efficient photocatalytic H_2 evolution over $Co(OH)_2$ modified CdS nanorods has not been reported up to date.

In this work, for the first time, we used the $Co(OH)_2$/CdS composites prepared by easy coprecipitation way for photocatalytic H_2 generation. To clarify the role of $Co(OH)_2$, photogenerated charge features of $Co(OH)_2$/CdS composites could are characterized by SPS, SPC, and transient photovoltage (TPV) techniques. A comprehensive explanation for the mechanism of enhanced photocatalytic H_2 evolution was proposed in terms of the role of $Co(OH)_2$. The study may be beneficial to developing inexpensive and efficient photocatalyst for water of decomposition.

EXPERIMENTAL SECTION

All the reagents are analytically pure. They are not further purified.

Synthesis of CdS Nanorods. CdS nanorods were synthesized with solvothermal way.[24] Typically, the cadmium nitrate tetrahydrate (4.66 g) was dispersed in reaction kettle with 72 mL of ethylenedi-

Received: February 27, 2014
Accepted: August 8, 2014
Published: August 8, 2014

amine containing thiourea (3.45 g). The solution was heated at 160 °C for 48 h and cooled down, spontaneously.

Synthesis of $Co(OH)_2$/CdS. The $Co(OH)_2$/CdS composites photocatalysts were prepared with easy coprecipitation strategy. Typically, CdS (0.4 g) was added into 0.25 M sodium hydrate solution (50 mL). Then 0, 1.3, 2.7, 4.6, 10.4, or 17.9 mL of 0.05 M $Co(NO_3)_2$ solution were dropwise put into above solution with stirring, respectively. After 2 h, the obtained composites were washed and then dried in vacuum. According to the results of ICP (as shown in Supporting Information Table S1), the theoretically loaded molar ratios of cobalt hydroxide to (cobalt hydroxide + cadmium sulfide) were R = 0, 1.7, 3.3, 6.8, 15, and 23 mol %. Therefore, those obtained composites were marked as S0, S1.7, S3.3, S6.8, S15, and S23, respectively. Pure cobalt hydroxide photocatalyst was synthesized using the above way without CdS.

Synthesis of Pt/CdS. A Pt/CdS composite was prepared by $NaBH_4$ reduction. In a typical procedure, CdS nanorods (0.4 g) were put into deionized water (50 mL) under stirring. Subsequently, 1.08 mL of H_2PtCl_6 aqueous solution (18.94 mmol/L) was injected. After it was stirred for 30 min, a $NaBH_4$ aqueous ($NaBH_4$/Pt = 10, molar ratio) was quickly put into the above solution. Then the solution was stirred for 1 h. The obtained composites were washed and dried.

Characterizations. The transmission electron microscopy(TEM; TECNAIG^2 FEI Company), high resolution transmission electron microscopy(HRTEM; TECNAIG^2 FEI Company) and field emission scanning electron microscopy(FESEM; FEI Company) are used to characterize morphologies and dimensions for photocatalysts. The X-ray diffraction (XRD) using Rigaku D/Max-2550 diffraction instrument with Cu Kα radialization (λ = 1.5418 Å, 50 kV, 200 mA) was used to characterize the crystallographic texture of photocatalyst. The scanning range of 2θ is from 10° to 70°. The scanning rate is 10° min^{-1}. The X-ray photoelectron spectroscopy (XPS) was conducted on the Thermo VG Scientific Escalab 250 spectrometer with monochromated Al Kα excitation source. In order to measure the absorption (300−800 nm), we have measured these dispersions on UV−vis-NIR Spectrophotometer (Shimadzu UV-3600). The surface photovoltage (SPV) and surface photocurrent (SPC) were carried out for investigating charges features on the previously reported equipment.[24,41] A self-made instrument[17] was used to investigate TPV features of photocatalysts. Briefly, a laser light eradiating impulse with 355 nm wavelength and 5 ns pulse width is as light resource; digital oscilloscope is as register. The ICP measurement was acquired on a PerkinElmer Optima 3300DV ICP spectrometer.

Electrochemical Measurements. The electrochemical H_2 generation feature of $Co(OH)_2$ was studied by a three electrodes system. Fluorine-doped tin oxide (FTO) electrode and FTO with $Co(OH)_2$ electrode were as the work electrodes. FTO electrode and $Co(OH)_2$/FTO electrode were as the work electrodes. The $Co(OH)_2$/FTO was made via dropping ethanol solution of $Co(OH)_2$ on FTO. 0.5 M Na_2SO_4 was used as electrolyte. Electrochemical measurements were conducted with CHI1630b electrochemical workstation. The Pt wire was used as counter electrode. The Ag/AgCl electrode was used as reference electrode.

Photocatalytic Reaction. A quartz container with 5.3 cm^2 of light coverage was used to test photocatalystic H_2 generation. The weight of sample was 0.1 g of 100 mL water solution including 25 mL ethanol was used as hole consumers. And the illumination time was 1 h, which was provided by 500 W xenon lamp. The gas phase chromatograph was employed to determine the concentration of H_2 evolution. The carrier gas was nitrogen (N_2).

RESULTS AND DISCUSSION

Figure 1 shows XRD patterns of CdS and $Co(OH)_2$/CdS composites, which can offer information about the crystallinity of photocatalysts. As can be seen in Figure 1, it is indicated that the samples have a pure phase of CdS. With increasing the concentration of $Co(OH)_2$, the diffraction peaks corresponding to (001) and (011) reflections of hexagonal β-$Co(OH)_2$ (PDF

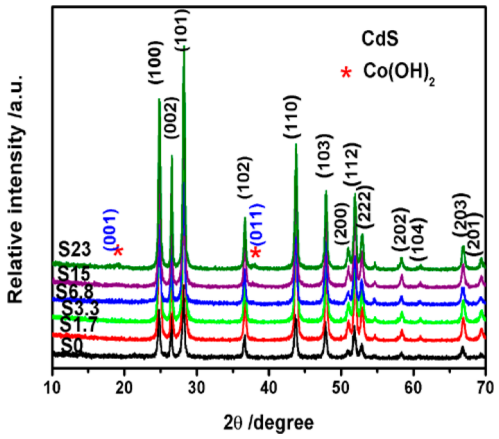

Figure 1. XRD patterns of $Co(OH)_2$/CdS with different molar percentages from 0% to 23%.

30-0443), are much more evident. The stars symbols are used to mark the XRD peaks of $Co(OH)_2$.

FESEM was used to characterize the morphology of S0, S6.8, and S15. Figure 2 exhibits CdS nanorods with diameters of

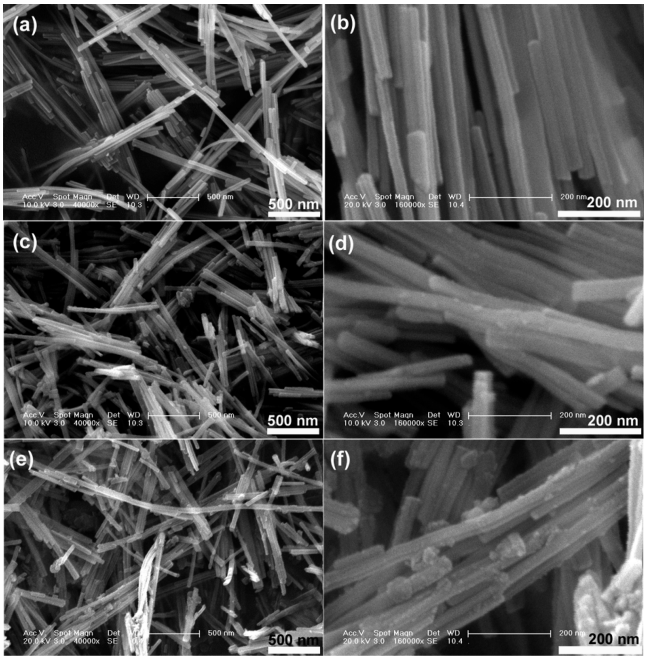

Figure 2. FESEM images of $Co(OH)_2$/CdS: (a and b) FESEM of S0, (c and d) the FESEM of 6.8, and (e and f) FESEM images of S15.

about 35 nm before and after loaded with $Co(OH)_2$. The surface of pure CdS nanorods seems neat and smooth (in Figure 2b). However, the surface of CdS nanorods becomes rougher with $Co(OH)_2$ loaded (in Figure 2(c, e). Besides, one can see (in Figure 2d, f) that there are many nanoparticles on the CdS nanorods. In Supporting Information Figure S1a, only Cd and S atoms could be detected in the EDAX of pure CdS, whereas the samples S6.8 and S15 contain Cd and S in addition to Co according to Supporting Information Figure S1c, d. On the basis of the results of XRD, FESEM, and EDAX, we deduce that the $Co(OH)_2$ nanoparticles have been successfully loaded on CdS.

The TEM could further provide information about surface features of $Co(OH)_2$/CdS composites.

One can observe that the surface of CdS nanorods is coated with many $Co(OH)_2$ nanoparticles with 2−10 nm, in Figure 3a, c. Figure 3b, d taken at interfacial region indicates that $Co(OH)_2$ nanometer particles were loaded on the hexagon CdS of single crystal. As can be seen in Figure 2b, d (corresponding to the square region marked in Figure 2a, c), the crystalline network for $Co(OH)_2$ could be recognized as the (100) interplanar distance of 0.27 nm. These results suggest that $Co(OH)_2$ nanoparticles are modified on CdS nanorods, which could be beneficial to electrons transfer between $Co(OH)_2$ and CdS. However, only a limited amount of $Co(OH)_2$ nanoparticles were observed on CdS nanorod surface in the TEM images. It is well-known that it is more difficult to load metal hydroxides and metal oxides on CdS than metal sulfides. According to recent reports, the loading amounts of metal sulfide cocatalysts are relatively smaller, for example, MoS_2 (0.2 wt %)/CdS,[15] NiS (1.2 mol %)/CdS,[26] and CuS (3 wt %)/CdS.[24] In contrast, herein for $Co(OH)_2$, the loading amount is up to 6.8 mol %. The following reasons may explain the discrepancy. Because S atom on CdS has low electronegativity(2.58) and large radius (0.104 nm), which make it difficult to form strong interaction (such as H-bond)[44] with H atom on $Co(OH)_2$. And the repulsive interaction between S atom and O atom is stronger than that between S atom and S atom which is not favor for loading cobalt hydroxide. Therefore, a certain of $Co(OH)_2$ separately aggregate into particles beyond CdS (as shown in the Supporting Information Figure S2 and Figure 2c, e). As a result, less $Co(OH)_2$ could grow on CdS. Therefore, it is no wonder that extra $Co(OH)_2$ is necessary in order to obtain effective H_2 evolution on $Co(OH)_2$/CdS photocatalyst. To determine the amount of $Co(OH)_2$, ICP, XPS, and EDAX are performed to check the molar ratios of cobalt hydroxide to (cobalt hydroxide + cadmium sulfide) (in Supporting Information Table S1). The

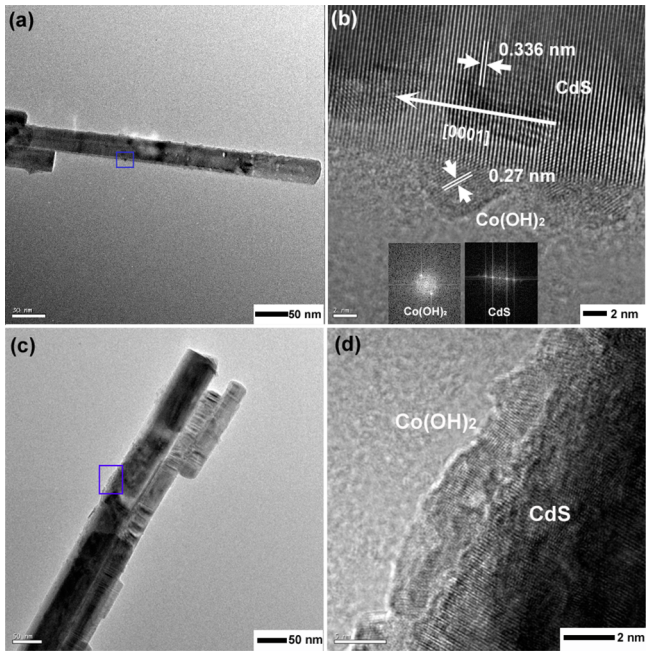

Figure 3. (a, c) TEM images of S6.8. (b, d) HRTEM images of S6.8. Inset of panel b shows the corresponding image by fast Fourier transform.

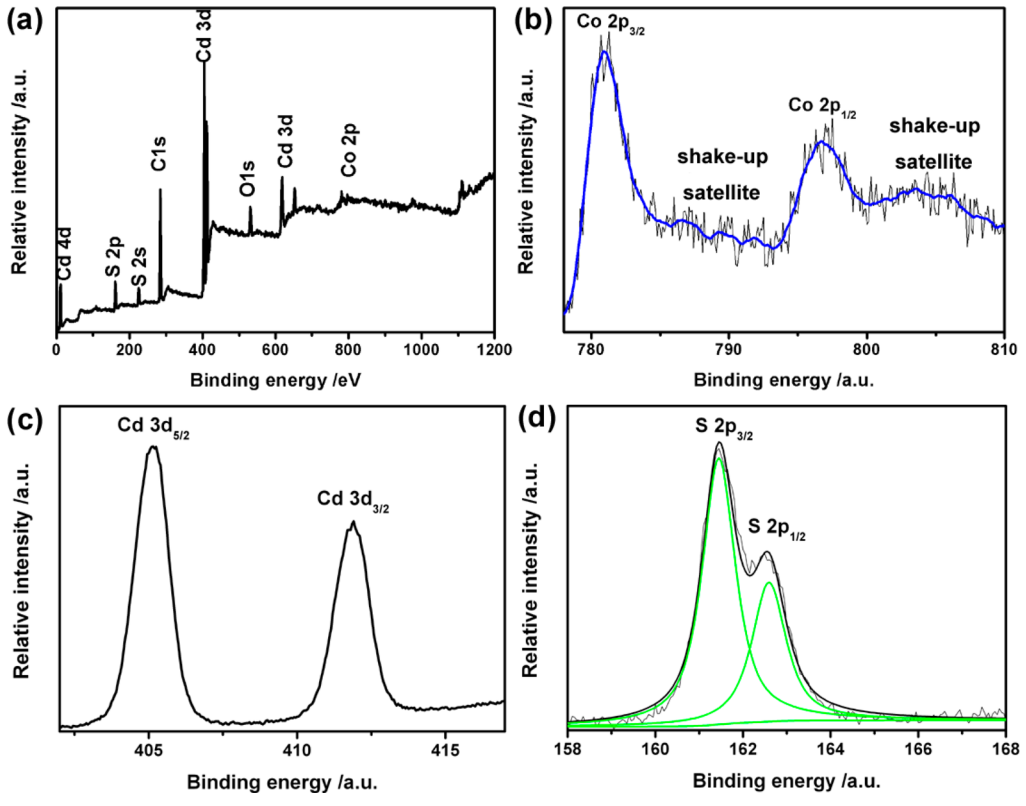

Figure 4. XPS spectra for the $Co(OH)_2$/CdS: (a) XPS survey spectrum of S6.8. (b−d) High resolution XPS spectra of Co 2p, Cd 3d, and S 2p.

results calculated from XPS, EDAX, and ICP are inconsistent. The molar ratios calculated from ICP are lower than feed ratios, while the molar ratios calculated from XPS and EDAX are higher than molar ratios calculated from ICP. This is caused by the following reason. The ICP can be used to analyze a variety of elements with high sensitivity and accurately detect the content of element in the whole sample. The results of ICP are lower than the feed ratios for loss in the course of experiment. The EDAX and XPS can be used for semiquantitative analysis and used to analyze the content of element on the surface of sample. Because $Co(OH)_2$ are mainly loaded on the surface of CdS, the results from EDXA and XPS are higher than that of the results of ICP.

The elements contained and states of Co element in sample S6.8 are further analyzed by XPS. Figure 4a shows that S6.8 contains cadmium, sulfur, oxygen, cobalt, and carbon elements. The peaks of C come from CO_2 adsorbed on the surface of photocatalyst and casual carbureted hydrogen adsorbed on XPS equipment.[21] The XPS spectrum for Co 2p of S6.8 (Figure 4b) shows the peaks at 796.7 and 781 eV, which are ascribed to Co $2p_{1/2}$ and Co $2p_{3/2}$ for Co^{2+} in $Co(OH)_2$.[22] Meanwhile, the distance in binding energies between Co $2p_{3/2}$ and Co $2p_{1/2}$ is about 16 eV, which is also indicative of presence of Co^{2+} in the form of $Co(OH)_2$.[23] The peaks of Cd $3d_{5/2}$ and $Cd_{3/2}$ can be observed at 405 and 412 eV, suggesting existence of Cd^{2+}.[24] This XPS spectrum of S 2p is shown in Figure 4d. The XPS signals of S 2p observed at around 162.6 eV (S $2p_{1/2}$) and 161.5 eV (S $2p_{3/2}$) are ascribed to S^{2-}, indicating the presence of metal sulfide.[25]

UV−vis diffuse reflectance spectra for S0, S1.7, S3.3, S6.8, S15, and S23 are shown in Figure 5. The absorption strength

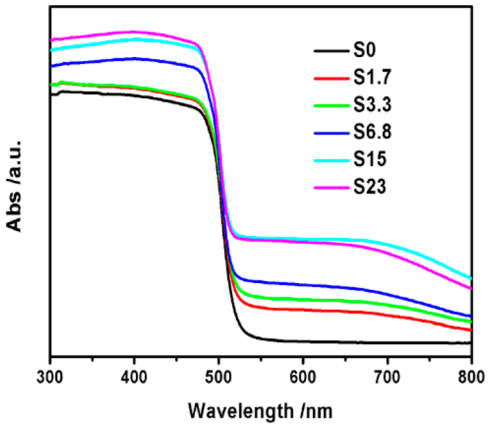

Figure 5. UV−vis diffuse reflectance spectra (UV−vis DRS) for $Co(OH)_2$/CdS nanocomposite with different $Co(OH)_2$/(CdS + $Co(OH)_2$) molar ratios from 0% to 23%.

for S0 (CdS) begins to rapidly raise at 518 nm, matching well with optical band gap absorption for pure CdS (2.4 eV). Meanwhile, compared with CdS, the increasing absorption (518−800 nm) can be obviously seen with increasing the content of $Co(OH)_2$. $Co(OH)_2$ alone exhibits an obvious absorption (300−800 nm) (in Supporting Information Figure S3). In addition, compared with CdS, the absorption edge of $Co(OH)_2$/CdS does not have evident shift, indicating that Co^{2+} did not enter crystal grating of CdS.[26]

No appreciable H_2 evolution could be obtained without illumination or photocatalyzer, indicating that H_2 generation is photoinduced reduction reaction over catalyst. As shown by the results in Figure 6, because photogenerated charges in CdS can easily recombine, CdS (S0) has low H_2 generation rate.

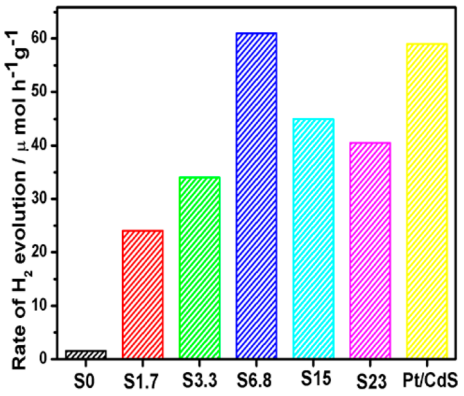

Figure 6. Photocatalytic H_2 generation rate over pure CdS, $Co(OH)_2$/CdS, and Pt/CdS samples.

Interestingly, little $Co(OH)_2$ deposited on CdS can evidently enhance H_2 generation rate of CdS. The sample S6.8 with 6.8 mol % of $Co(OH)_2$ exhibits the highest H_2 evolution rate of 61 μmol $h^{-1}g^{-1}$, showing around 41 higher than H_2 generation rate of S0 (CdS). Compared with Pt (1 wt %)/CdS, S6.8 also shows higher H_2 generation rate. However, redundant $Co(OH)_2$ leads to decrease of H_2 evolution rate. The following two factors probably account for the negative role of excess $Co(OH)_2$: (I) Too much $Co(OH)_2$ loaded can keep light from CdS, which could result in reducing light absorption of CdS and the number of photogenerated charges in CdS. (II) Superfluous $Co(OH)_2$ could become deathnium, which could cause reduction of photocatalytic H_2 generation rate.[27] What' s more, $Co(OH)_2$ alone does not show any photocatalystic H_2 generation activity at same test conditions. Using the UV−vis source herein, the H_2 evolution rate of $Co(OH)_2$/CdS appears to be higher than those reported for p-MoS_2/n-RGO,[28] NGO-QDs,[29] Pt−Au−WO_3,[30] $BiVO_4$/Ru-$SrTiO_3$:Rh,[31] CdSe in 20% CH_3OH(aq),[32] Pt-IrO_2/WO_3//Dye-absorbed Pt/$H_4Nb_6O_{17}$,[33] NiO_x/$K_4Ce_2M_{10}O_3$ (M = Ta, Nb),[34] Pt-WO_3/Pt-$SrTiO_3$(Cr, Ta),[35] and PtATaO_2N(A: Ca, Sr, Ba)/WO_3,[36] but lower than those reported for MoS_2/CdS[15] and WS_2/CdS,[16] which are tested in a wide range of conditions in the literature although light frequency, intensity irradiation area and so on should be the same for a fairer comparison. We also studied the photocatalytic H_2 evolution activity of $Co(OH)_2$/CdS with visible radiation, and S6.8 also exhibits the highest H_2 evolution rate (in Supporting Information Figure S4).

To design effective photocatalysts used to produce H_2 from water of decomposition, it is necessary and important to fully understand the charges transmission at interface.[37] Therefore, SPC and SPV were used to research photogenerated charges transmission features of $Co(OH)_2$/CdS, which could be beneficial for understanding the effect of $Co(OH)_2$. Because of separation of photogenerated charges in space, the SPV signal arises.[38] Figure 7a shows the SPV spectra of S0, S3.3, S6.8, and S15. There are two evident SPV responses in the SPV spectrum of S0. The positive SPV signal in the 300−518 nm corresponds to band-to-band transition of CdS, which reveals photogenerated electrons transfer to bulk and photogenerated holes to surface.[39] This is representative feature of n-type semiconductor in SPV, where positive charges of surface space charges area migrate to the surface.[40] This sub-band transition

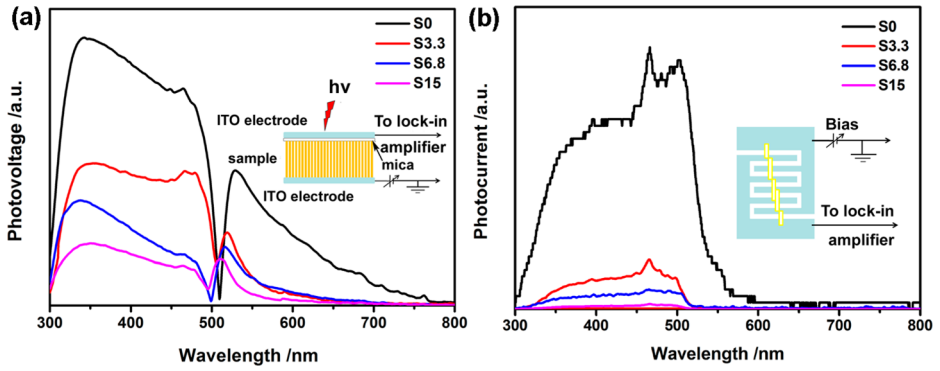

Figure 7. (a) SPV spectra of S0, S3.3, S6.8 and S15. Inset shows the schematic setup of SPS measurement. (b) SPC spectra of S0, S3.3, S6.8, and S15. Inset shows the schematic setup of SPC measurement.

of CdS corresponds to SPV response in 518−800 nm. Compared with S0, the SPV signals of $Co(OH)_2$/CdS in the range of 300−518 nm is reduced clearly. This may be caused by two reasons. The first reason is that $Co(OH)_2$ loaded on CdS could prevent CdS from absorbing light and reduce the number of photogenerated charges. However, this is not consistent with the results of photocatalytic H_2 evolution. So this reason is not main reason for reduction of SPV signal for $Co(OH)_2$/CdS. The second reason is that $Co(OH)_2$ loaded on the surface of CdS acts as an electron acceptor, which could offset some part of the positive photoelectric signal and result in reduction of SPV signal for $Co(OH)_2$/CdS. More photogenerated electrons are accumulated on surface of CdS, which is beneficial for photocatalytic reduction. And it will result in the enhanced photocatalytic H_2 evolution rate. Thus, the second reason is main reason for reduction of photoelectric signal for $Co(OH)_2$/CdS. The S15 has the lowest SPV signal while the photocatalytic H_2 evolution rate of S15 is lower than that of S6.8. This may mainly be caused by the fist reason. Too much $Co(OH)_2$ coated could prevent light absorption, reduce the number of photogenerated charges and reduce the chance that photogenerated holes in CdS take part in the photocatalytic oxidation reaction with ethanol, which inevitably causes the decrease of the photocatalytic H_2 evolution rate. So the $Co(OH)_2$ have a best load. Figure 7b shows the SPC spectra of S0, S3.3, S6.8, and S15. The SPC response intensity of $Co(OH)_2$/CdS is weaker than that of pure CdS, which indicates that $Co(OH)_2$ loaded acts as electron acceptors.[24,41] With the increase of $Co(OH)_2$ loaded, more photogenerated electrons of CdS are captured, which could cause the decrease of the amount of photogenerated electrons in CdS, block the horizon transfer of photogenerated electrons and cause the reduction of SPC. Too much $Co(OH)_2$ which is coated on CdS could prevent light absorption. Thus, the photocatalytic H_2 evolution rate of S15 is lower than that of S6.8.

TPV spectrum could reflect photophysical processes (transmission and separation) of photogenerated charges in samples. Therefore, TPV tests were adopted. Figure 8 shows the TPV spectra of S0, S3.3, S6.8, and S15 under 355 nm light irradiation. Two interesting features can be obtained: (I) All photocatalysts show positive TPV signals, which indicate n-type feature of CdS. (II) Two peaks are obtained in the TPV response for $Co(OH)_2$/CdS, the P1 peak located at time $<10^{-6}$ s and P2 peak located at time $>10^{-4}$ s. When laser burst acts on samples, photogenerated charges separate because of the effect of electric field of space charge zone. Then, TPV response goes up in the rage of $0-10^{-6}$ s.[39] Because of the effect of $Co(OH)_2$,

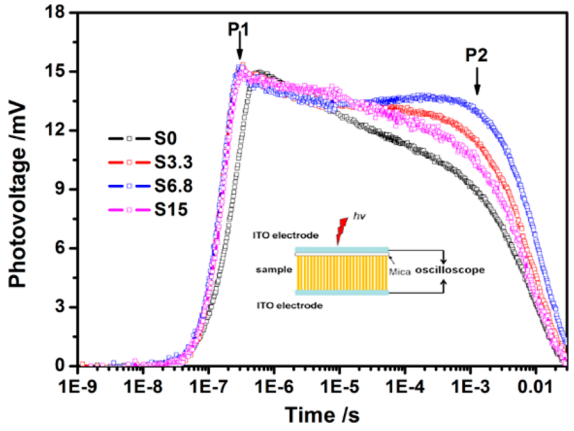

Figure 8. Normalized TPV spectra of S0, S3.3, S6.8, and S15. Inset shows the schematic setup of TPV measurement.

which can capture photogenerated electrons in CdS, the photogenerated charges can quickly separate in $Co(OH)_2$/CdS, which is faster than photogenerated charge separation in pure CdS. So the P1 peak arises earlier for $Co(OH)_2$ cocatalyst loaded compared with pure CdS. When the time is longer than 1×10^{-4}, an obvious retardation peak (P2) corresponding to diffusion photovoltage[42] can be obtained in the TPV of $Co(OH)_2$/CdS. Yet, no obvious retardation peak can be observed for S0. The time corresponding retarded peak is a balance point at which recombination rate of photogenerated charges is equal to separation rate. The numerial number of time corresponding to P2 is larger. Then, the photogenerated charges would need longer time to recombine. This indicates that generated electrons could have more chances to take part in the reaction of H_2 evolution from water of decomposition. So, $Co(OH)_2$ loaded increased separation efficiency of photogenerated charges and inhibited the recombination of photogenerated charges and inhibited the recombination of photogenerated charges. There is no doubt that they could result in increasing of H_2 generation rate of $Co(OH)_2$/CdS. What's more, the sample S6.8 has most obvious retardation peak P2, which indicates that the sample S6.8 has maximum separation efficiency of photogenerated charges. So the sample S6.8 has the highest photocatalytic H_2 evolution rate.

Figure 9 shows the polarization curves for FTO and FTO with $Co(OH)_2$, with increasing potential. FTO shows cathode current associated with H_2 generation. However, compared with FTO, $Co(OH)_2$/FTO shows enhanced cathode current at same potential. The cathode current of FTO with $Co(OH)_2$ is

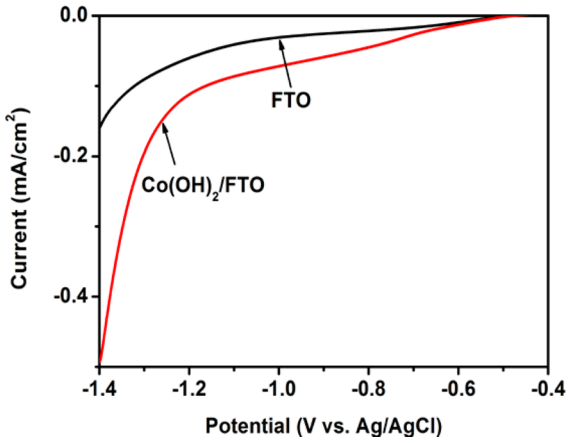

Figure 9. Polarization curves of FTO with and without $Co(OH)_2$ in 0.5 M Na_2SO_4 solution.

3 times higher than current of FTO at −1.4 V versus Ag/AgCl electrode. Thus, $Co(OH)_2$ as a nice catalyst could be used to catalyze H_2 generation. This is regarded as a vital factor for enhancement of photocatalystic H_2 generation for $Co(OH)_2$/CdS.[43]

CONCLUSION

In summary, the photocatalytic H_2 generation of CdS can be obviously increased by coating $Co(OH)_2$ cocatalyst. The $Co(OH)_2$(6.8 mol %)/CdS shows highest H_2 generation rate of 61 μmol h^{-1} g^{-1}, which runs 41 times as high as rate of CdS. What is more, S6.8 expresses higher activity than CdS with Pt cocatalyst. Electrons captured by $Co(OH)_2$ is leading cause for increase of H_2 generation rate over CdS. Electrons caught not only improve charges separation in CdS but also make more electrons take part in reduction. The research could be in favor of designing abundant and efficient catalysts for water of decomposition.

ASSOCIATED CONTENT

Supporting Information

XRD pattern of $Co(OH)_2$, UV−vis DRS of $Co(OH)_2$, the EDAX of S0, S6.8, and S15, the TEM of S15, and the rate of H_2 evolution over $Co(OH)_2$/CdS under visible light. This material is available free of charge via the Internet at http://pubs.acs.org.

AUTHOR INFORMATION

Corresponding Authors

*E-mail: ltlwll98003082@aliyan.com.
*E-mail: xietf@jlu.edu.cn.

Notes

The authors declare no competing financial interest.

ACKNOWLEDGMENTS

This research was supported by the Nation Basic Research program of china (973 program) (2013CB632403), the National Natural Science Foundation of China (no. 21173103) and the National Natural Science Foundation of China (no. 51172090).

REFERENCES

(1) Ong, W.; Gao, M.; Ho, G. Hybrid Organic PVDF−Inorganic M-rGO-TiO_2 (M = Ag, Pt) Nanocomposites for Multifunctional Volatile Organic Compound Sensing and Photocatalytic Degradation-H_2 Production. *Nanoscale* **2013**, *5*, 11283−11290.
(2) Feng, L.; Zou, X.; Zhao, J.; Zhou, L.; Wang, D.; Zhang, X.; Li, G. Nanoporous Sr-Rich Strontium Titanate: A Stable and Superior Photocatalyst for H_2 Evolution. *Chem. Commun.* **2013**, *49*, 9788−9790.
(3) Kong, D.; Cha, J.; Wang, H.; Lee, H.; Cui, Y. First-Row Transition Metal Dichalcogenide Catalysts for Hydrogen Evolution Reaction. *Energy Environ. Sci.* **2013**, *6*, 3553−3558.
(4) Sim, U.; Yang, T.; Moon, J.; An, J.; Hwang, J.; Seo, J.; Lee, J.; Kim, K.; Lee, J.; Han, S.; Hong, B.; Nam, K. N-Doped Monolayer Graphene Catalyst on Silicon Photocathode for Hydrogen Production. *Energy Environ. Sci.* **2013**, *6*, 3658−3664.
(5) Moriya, M.; Minegishi, T.; Kumagai, H.; Katayama, M.; Kubota, J.; Domen, K. Stable Hydrogen Evolution from CdS-Modified $CuGaSe_2$ Photoelectrode under Visible-Light Irradiation. *J. Am. Chem. Soc.* **2013**, *135*, 3733−3735.
(6) Lingampalli, S.; Gautam, U.; Rao, C. Highly Efficient Photocatalytic Hydrogen Generation by Solution-processed ZnO/Pt/CdS, ZnO/Pt/$Cd_{1-x}Zn_xS$ and ZnO/Pt/$CdS_{1-x}Se_x$ Hybrid Nanostructures. *Energy Environ. Sci.* **2013**, *6*, 3589−3594.
(7) Jia, L.; Wang, D.; Huang, Y.; Xu, A.; Yu, H. Highly Durable N-Doped Graphene/CdS Nanocomposites with Enhanced Photocatalytic Hydrogen Evolution from Water under Visible Light Irradiation. *J. Phys. Chem. C* **2011**, *115*, 11466−11473.
(8) Xu, Y.; Zhao, W.; Xu, R.; Shi, Y.; Zhang, B. Synthesis of Ultrathin CdS Nanosheets as Efficient Visible-Light-Driven Water Splitting Photocatalysts for Hydrogen Evolution. *Chem. Commun.* **2013**, *49*, 9803−9805.
(9) Yan, H.; Yang, J.; Ma, J. G.; Wu, G.; Zong, X.; Li, C. Visible-Light-Driven Hydrogen Production with Extremely High Quantum Efficiency on Pt-PdS/CdS Photocatalyst. *J. Catal.* **2009**, *266*, 165−168.
(10) Berr, M.; Vaneski, A.; Susha, A.; Rodríguez-Fernández, J.; Döblinger, M.; Jäckel, F.; Rogach, A.; Feldmann, J. Colloidal CdS Nanorods Decorated with Subnanometer Sized Pt Clusters for Photocatalytic Hydrogen Generation. *J. Appl. Phys. Lett.* **2010**, *97*, No. 093108.
(11) Li, Q.; Guo, B.; Yu, J.; Ran, J.; Zhang, B.; Yan, H.; Gong, J. Highly Efficient Visible-Light-Driven Photocatalytic Hydrogen Production of CdS-Cluster-Decorated Graphene Nanosheets. *J. Am. Chem. Soc.* **2011**, *133*, 10878−10884.
(12) Yan, H.; Yang, J.; Ma, G.; Wu, G.; Zong, X.; Li, C. Visible-Light-Driven Hydrogen Production with Extremely High Quantum Efficiency on Pt-PdS/CdS Photocatalyst. *J. Catal.* **2009**, *266*, 165−168.
(13) Yu, J.; Ran, J. Facile Preparation and Enhanced Photocatalytic H_2-Production Activity of $Cu(OH)_2$ Cluster Modified TiO_2. *J. Energy Environ. Sci.* **2011**, *4*, 1364−1371.
(14) Zhou, J.; Tian, G.; Chen, Y.; Meng, X.; Shi, Y.; Gao, X.; Pan, K.; Fu, H. In Situ Controlled Growth of $ZnIn_2S_4$ Nanosheets on Reduced Graphene Oxide for Enhanced Photocatalytic Hydrogen Production Performance. *Chem. Commun.* **2013**, *49*, 2237−2239.
(15) Zong, X.; Yan, H.; Wu, G.; Ma, G.; Wen, F.; Wang, L.; Li, C. Enhancement of Photocatalytic H_2 Evolution on CdS by Loading MoS_2 as Cocatalyst under Visible Light Irradiation. *J. Am. Chem. Soc.* **2008**, *130*, 7176−7177.
(16) Zong, X.; Han, J.; Ma, G.; Yan, H.; Wu, G.; Li, C. Photocatalytic H_2 Evolution on CdS Loaded with WS_2 as Cocatalyst under Visible Light Irradiation. *J. Phys. Chem. C* **2011**, *115*, 12202−12208.
(17) Zhang, L.; Jiang, T.; Li, S.; Lu, Y.; Wang, L.; Zhang, X.; Wang, D.; Xie, T. Enhancement of Photocatalytic H_2 Evolution on $Zn_{0.8}Cd_{0.2}S$ Loaded with CuS as Cocatalyst and Its Photogenerated Charge Transfer Properties. *Dalton Trans.* **2013**, *42*, 12998−13003.
(18) Mondal, C.; Ganguly, M.; Manna, P.; Yusuf, S.; Pal, T. Fabrication of Porous β-$Co(OH)_2$ Architecture at Room Temperature: A High Performance Supercapacitor. *Langmuir* **2013**, *29*, 9179−9187.
(19) Zhang, Y.; Cui, B.; Qin, Z.; Lin, H.; Li, J. Hierarchical Wreath-Like Au-$Co(OH)_2$ Microclusters for Water Oxidation at Neutral pH. *Nanoscale* **2013**, *5*, 6826−6833.

(20) Elumalai, P.; Vasan, H.; Munichandraiah, N. Electrochemical Studies of Cobalt Hydroxide—An Additive for Nickel Electrodes. *J. Power Sources* **2001**, *93*, 201−208.
(21) Yu, J.; Hai, Y.; Cheng, B. Enhanced Photocatalytic H_2-Production Activity of TiO_2 by $Ni(OH)_2$ Cluster Modification. *J. Phys. Chem. C* **2011**, *115*, 4953−4958.
(22) Yang, J.; Sasaki, T. Synthesis of CoOOH Hierarchically Hollow Spheres by Nanorod Self-Assembly through Bubble Templating. *Chem. Mater.* **2008**, *20*, 2049−2056.
(23) Dillard, J.; Schenck, C.; Koppelmon, M. Surface Chemistry of Cobalt in Calcined Cobalt-Kaolinite Materials. *Clays Clay Miner.* **1983**, *31*, 69−72.
(24) Zhang, L.; Xie, T.; Wang, D.; Li, S.; Wang, L.; Chen, L.; Lu, Y. Noble-Metal-Free CuS/CdS Composites for Photocatalytic H_2 Evolution and Its Photogenerated Charge Transfer Properties. *Int. J. of Hydrogen Energy* **2013**, *38*, 11811−11817.
(25) Moulder, J.; Stickle, W.; Sobol, P.; Bomben, K. *Handbook of X-ray Photoelectron Spectroscopy*; Physical Electronics, Inc.: Eden Prairie, MN, 1992; pp 1−190.
(26) Zhang, W.; Wang, Y.; Wang, Z.; Zhong, Z.; Xu, R. Highly Efficient and Noble Metal-Free NiS/CdS Photocatalysts for H_2 Evolution from Lactic Acid Sacrificial Solution under Visible Light. *Chem. Commun.* **2010**, *46*, 7631−7633.
(27) Zhang, J.; Yu, J.; Jaroniec, M.; Gong, J. Noble Metal-Free Reduced Graphene Oxide-$Zn_xCd_{1-x}S$ Nanocomposite with Enhanced Solar Photocatalytic H_2-Production Performance. *Nano Lett.* **2012**, *12*, 4584−4589.
(28) Meng, F.; Li, J.; Cushing, S.; Zhi, M.; Wu, N. Solar Hydrogen Generation by Nanoscale p−n Junction of p-Type Molybdenum Disulfide/n-Type Nitrogen-Doped Reduced Graphene Oxide. *J. Am. Chem. Soc.* **2013**, *135*, 10286−10289.
(29) Yeh, T.; Teng, C.; Chen, S.; Teng, H. Nitrogen-Doped Graphene Oxide Quantum Dots as Photocatalysts for Overall Water-Splitting under Visible Light Illumination. *Adv. Mater.* **2014**, *26*, 3297−3303.
(30) Tanaka, A.; Hashimoto, K.; Kominami, H. Visible-Light-Induced Hydrogen and Oxygen Formation over $Pt/Au/WO_3$ Photocatalyst Utilizing Two Types of Photoabsorption Due to Surface Plasmon Resonance and Band-Gap Excitation. *J. Am. Chem. Soc.* **2014**, *136*, 586−589.
(31) Sasaki, Y.; Kato, H.; Kudo, A. $[Co(bpy)3]^{3+/2+}$ and $[Co(phen)_3]^{3+/2+}$ Electron Mediators for Overall Water Splitting under Sunlight Irradiation Using Z-Scheme Photocatalyst System. *J. Am. Chem. Soc.* **2013**, *135*, 5441−5449.
(32) Frame, F.; Carroll, E.; Larsen, D.; Sarahan, M.; Browning, N.; Osterloh, F. First Demonstration of CdSe as A Photocatalyst for Hydrogen Evolution from Water under UV and Visible Light. *Chem. Commun.* **2008**, 2206−2208.
(33) Abe, R.; Shinmei, K.; Koumura, N.; Hara, K.; Ohtani, B. Visible-Light-Induced Water Splitting Based on Two-Step Photoexcitation between Dye-Sensitized Layered Niobate and Tungsten Oxide Photocatalysts in the Presence of a Triiodide/Iodide Shuttle Redox Mediator. *J. Am. Chem. Soc.* **2013**, *135*, 16872−16884.
(34) Shangguan, W. Hydrogen Evolution from Water Splitting on Nanocomposite Photocatalysts. *Sci. Technol. Adv. Mater.* **2007**, *8*, 76−81.
(35) Sayama, K.; Mukasa, K.; Abe, Y.; Arakama, H. A New Photocatalytic Water Splitting System under Visible Light Irradiation Mimicking A Z-scheme Mechanism in Photosynthesis. *J. Photochem. Photobiol., A* **2002**, *148*, 71−77.
(36) Higashi, M.; Abe, R.; Teramura, K.; Takata, T.; Ohtani, B.; Domen, K. Two Step Water Splitting into H_2 and O_2 under Visible Light by $ATaO_2N$ (A = Ca, Sr, Ba) and WO_3 with Shuttle Redox Mediator. *Chem. Phys. Lett.* **2008**, *452*, 120−123.
(37) Kamat, P. TiO_2 Nanostructures: Recent Physical Chemistry Advances. *J. Phys. Chem. C* **2012**, *116*, 11849−11851.
(38) Mora-sero, I.; Dittrich, T.; Belaidi, A.; Crarcia-belmonte, G.; Bisquert, J. Observation of Diffusion and Tunneling Recombination of Dye-Photoinjected Electrons in Ultrathin TiO_2 Layers by Surface Photovoltage Transients. *J. Phys. Chem. B* **2005**, *109*, 14932−14938.
(39) Kronik, L.; Shapira, Y. Surface Photovoltage Phenomena: Theory, Experiment, and Applications. *Surf. Sci. Rep* **1999**, *37*, 1−206.
(40) Timoshenko, V.; Duzhko, V.; Dittrich, T. Diffusion Photovoltage in Porous Semiconductors and Dielectrics. *Phys. Status Solidi A* **2000**, *182*, 227.
(41) Wang, P.; Xie, T.; Li, H.; Peng, L.; Zhang, Y.; Wu, T. Synthesis and Plasmon-Induced Charge-Transfer Properties of Monodisperse Gold-Doped Titania Microspheres. *Chem.—Eur. J.* **2009**, *15*, 4366−4372.
(42) Timoshenko, V. Y.; Duzhko, V.; Dittrich, T. Diffusion Photovoltage in Porous Semicon ductors and Dielectrics. *Phys. Status Solidi A* **2000**, *182*, 227.
(43) Zong, X.; Wu, G.; Yan, H.; Ma, G.; Shi, J.; Wen, F.; Wang, L.; Li, C. Photocatalytic H_2 Evolution on MoS_2/CdS Catalysts under Visible Light Irradiation. *J. Phys. Chem. C* **2010**, *114*, 1963−1968.
(44) Ran, J.; Yu, J.; Jaroniec, M. $Ni(OH)_2$ Modified CdS Nanorods for Highly Efficient Visible-Light-Driven Photocatalytic H_2 Generation. *Green Chem.* **2011**, *13*, 2708−2713.